

RESEARCH

Open Access



A tailored bioactive 3D porous poly(lactic-acid)-exosome scaffold with osteo-immunomodulatory and osteogenic differentiation properties

Yi Zhang^{1†}, Mengjie Huo^{2†}, Yi Wang², Lan Xiao^{3,4}, Jianmei Wu², Yaping Ma², Dingmei Zhang², Xuemei Lang^{5*} and Xin Wang^{1,2,3,4*}

Abstract

Polylactic acid (PLA) is a versatile and biodegradable scaffold widely used in biomedical fields to repair tissue defects. Exosomes derived from mesenchymal stem cells (MSCs) are nano-sized extracellular vesicles, which play an important role in tissue engineering in recent years. The primary focus of this study was to develop a bioactive 3D PLA scaffold using exosome-based strategy to improve its osteogenic and immunoregulatory potential. We firstly successfully isolated MSC-derived exosomes (MSC-Exo). Morphological analysis revealed that MSC-Exo exhibits a typical cup-shaped morphology with high expression of exosomal marker CD63. MSC-Exo internalization into recipient cells were also investigated using flow cytometry and confocal laser scanning microscopy. Porous 3D PLA scaffold coated MSC-Exo were used for immunoregulatory and osteogenic testing. Exosomes released from 3D PLA scaffold were validated in RAW264.7 and hBMSCs. The cell proliferation and live/dead assay indicated high biocompatibility for PLA-Exo scaffold. Additionally, PLA-Exo scaffold could reduce the pro-inflammatory marker expression and reactive oxygen species (ROS) production, indicating potential immunoregulatory potential. It is also confirmed that PLA-Exo scaffold could potentiate osteogenic differentiation in the osteogenesis assay. In conclusion, our results demonstrate this bioactive 3D-printed PLA scaffolds with MSC-Exo modification holds immunoregulatory potential and favor osteogenic differentiation, thus having potential applications in bone tissue regeneration.

Keywords: MSC-Exo, Bioactive 3D PLA scaffold, Macrophages, Immunoregulation, Osteogenesis

Introduction

Large bone defects or non-union bone fractures caused by musculoskeletal tumors, traumatic injury, or under various pathological conditions, represent a fundamental challenge for orthopedic surgeons [1]. To date, various reconstructive options, including autologous iliac grafting, allogeneic bone graft, induced membrane technique, as well as using various bioactive materials, have gained acceptance in orthopedic practice to treat large bone defects [2]. Autografts containing native tissues and a vascularization bed remain the gold standard technique to reconstruct large bone defect due to

[†]Yi Zhang and Mengjie Huo contributed equally to this work and are considered co-first authors.

*Correspondence: 609881611@qq.com; lchwx@aliyun.com

²Department of Orthopaedic Surgery, Affiliated Hospital of Zunyi Medical University, Zunyi 563003, Guizhou, China

⁵Department of Pre-hospital Emergency, Central Hospital of Chongqing University / Chongqing Emergency Medical Center, Chongqing, Chongqing 400014, China

Full list of author information is available at the end of the article



© The Author(s) 2022. **Open Access** This article is licensed under a Creative Commons Attribution 4.0 International License, which permits use, sharing, adaptation, distribution and reproduction in any medium or format, as long as you give appropriate credit to the original author(s) and the source, provide a link to the Creative Commons licence, and indicate if changes were made. The images or other third party material in this article are included in the article's Creative Commons licence, unless indicated otherwise in a credit line to the material. If material is not included in the article's Creative Commons licence and your intended use is not permitted by statutory regulation or exceeds the permitted use, you will need to obtain permission directly from the copyright holder. To view a copy of this licence, visit <http://creativecommons.org/licenses/by/4.0/>. The Creative Commons Public Domain Dedication waiver (<http://creativecommons.org/publicdomain/zero/1.0/>) applies to the data made available in this article, unless otherwise stated in a credit line to the data.

its inherent osteoinductive and biocompatible properties [3, 4]. However, the main disadvantages are labor-intensive surgery, limited sources, and possible donor site complications [4]. The incident of non-union bone fractures will continue to rise with the aging populations, thus causing huge social and economic burdens.

Exosomes (Exo), with an average size of 40–160 nm, are a type of extracellular vesicles secreted by most eukaryotic cells [5]. Since its discovery in 1980s, exosomes have attracted increasing attentions in recent years to contribute intercellular communication under various physiological and pathological conditions [6]. Surrounded by a lipid bilayer membrane, exosomes are functional vehicles that carry a bioactive cargo of proteins, nucleic acids (DNA, mRNA, microRNA, circular RNA), lipids, and metabolites, etc., which play an important role in reprogramming recipient cell function and behavior [7]. In recent years, therapeutic intervention mediated by exosomes with immunomodulatory properties have attracted increasing attentions to accelerate skeletal tissue repair. Mesenchymal stem cells (MSCs) are nonhematopoietic fibroblast-like multipotent adult stem cells derived from adult tissues with self-renewal potential [8]. Over the past decades, the application of exogenous bone marrow derived MSCs, along with other bioactive molecules, and composite scaffolds, have exhibited enormous potential for regenerating skeletal tissue [9, 10]. Additionally, therapeutic intervention mediated by exosomes from MSCs, are being explored as novel cell-free alternative to cellular therapy in regenerative medicine [11]. Administration of MSCs derived exosomes has been reported to be efficacious in promoting skeletal muscle regeneration [12], cartilage repair [13], and bone fracture healing [14], and cutaneous wound healing [15]. Additionally, the broad-spectrum therapeutic efficacy of MSC-derived exosomes have also been validated in multiple disease models, including carbon tetrachloride (CCl₄)-induced liver injury [16], myocardial ischemia/reperfusion injury [17], LPS-induced acute respiratory distress syndrome [18], and graft-versus-host disease [19].

Numerous biocompatible and biodegradable polymeric materials, such as polycaprolactone (PCL), poly(acrylonitrile butadiene styrene) (ABS), polylactic acid (PLA), and polyglycolic acid (PGA), etc. are widely used in the field of regenerative medicine [20]. PLA has been increasingly utilized to construct 3D-printed bone implants [21]. Despite its mechanical stability, and cytocompatibility advantage, further surface modification is still needed to increase its bioactivity. In this study, we developed an exosome-based surface modification strategy to modify the PLA surface to improve its osteogenic

and immunoregulatory potential. Our results indicate that PLA/MSC-Exo scaffold may serve as a potential therapeutic scaffold for hard tissue regeneration.

Materials and methods

Cell culture and exosome isolation

To obtain exosomes, the human bone marrow-derived mesenchymal stromal cells (hBMSCs, ATCC® PCS-500-012™) were used in this study. Cells were cultured in Dulbecco's Modified Eagle's Medium (DMEM; Life Technologies Pty Ltd., China) supplemented with 10% fetal bovine serum (FBS; Biological Industries, LTD, Beit Haemek, Israel), and 1% (v/v) penicillin/streptomycin (Solarbio, Beijing, China) in atmosphere of 5% CO₂ at 37°C. For conditioned medium (CM) collection, hBMSCs (passage 3) were seeded in T75 flasks and were cultured to 90% confluence at 37°C. After rinsing thrice with phosphate-buffered saline (PBS), cells were cultured with 10 mL DMEM supplemented with 10% exosome-depleted FBS at 37°C for 24 h in order to collect CM [22]. The collected CM was pooled together before exosomes isolation. Exosomes were isolated according to published guidelines [23]. First, CM was filtered through 0.22 μm filters to remove live cells and other large membranous structures. Second, CM was centrifuged at 300×g at 4°C for 10 min to pellet any remaining live cells. Third, CM was transferred to new tubes and centrifuged at 2,000×g at 4°C for 20 min. Then the CM was centrifuged in a 45Ti rotor (Beckman) at 10,000×g at 4°C for 40 min. The supernatant was spun at 100,000×g at 4°C for 90 min to pellet exosomes. The exosome pellets were resuspended in PBS, aliquoted and stored at –80°C immediately until further analysis.

Transmission electron microscopy (TEM)

Exosomes (5 μL) were mounted on TEM copper grids (200 mesh and coated by formvar carbon film) for 5 min at room temperature and stained with 1% uranyl acetate for 20 s. Excess uranyl acetate was removed by rinsing with deionized water and samples were dried using Whatman filter paper before imaging. A JEM-1400, JOEL TEM was used to image exosome samples at a voltage of 80 kV.

Western blot

To identify the exosome marker, samples were resuspended in RIPA lysis buffer and analyzed by Western blot. Proteins were separated using 10% sodium dodecyl sulfate-polyacrylamide gel electrophoresis (SDS-PAGE) and transferred to a polyvinylidene difluoride (PVDF) membrane. The membrane was blocked with Odyssey® Blocking Buffer (LI-COR Biotechnology, USA) for 1 h. Membranes were incubated with the following primary

antibody: Anti-CD63 Antibody (E-12) (1:100, sc-365,604, Santa Cruz). The following secondary antibody was used: IRDye® 680RD goat anti-mouse IgG (H+L) (1:10,000; LI-COR Biotechnology, USA). The protein signal intensity was detected using Odyssey infrared Imaging System (LI-COR Biotechnology, USA).

Exosome labeling and cellular uptake of exosomes

Exosome labeling was performed using PKH26 red fluorescent cell linker kit for general cell membrane labeling according to the manufacturer's instruction (PKH26GL-1KT, Sigma, China). PKH26-labeled exosomes were incubated with recipient cells for 24 h at 37°C. After treatment, cells were washed with PBS twice, trypsinized using 0.25% trypsin-EDTA, and analyzed using a BD Caliber flow cytometer. The mean fluorescence intensity (MFI) was calculated according to the flow cytometry data.

For fluorescence imaging, cells were washed with PBS, fixed with 4% paraformaldehyde, permeabilized using 0.25% Triton, and stained with Alexa Fluor 488-labeled phalloidin in dark for 1 h followed by DAPI staining. Images were captured using a confocal laser scanning microscope with a $\times 40$ objective (Leica DM IRB; Leica, Wetzlar, Germany).

Preparation of porous PLA and MSC-Exo scaffolds

The patterns for 3D printed scaffolds were designed using AutoCAD software (Autodesk, Inc., San Rafael, CA, USA) and saved as stereolithography (.stl) file. PLA filament (diameter 1.75 mm) was used to fabricate layer-by-layer 3D scaffolds with a customized 3D printer as described previously [21]. Briefly, PLA filament (1.75 mm diameter) was fed directly into the printer head and extruded via the printing nozzle at 200°C. The scaffolds were printed with a 10 mm diameter, 4 mm height with a pore diameter of $\sim 500 \mu\text{m}$. Poly(dopamine)-based surface modification technique was used to firstly modify the PLA scaffold based on our previous studies [22, 24]. Briefly, poly(dopamine) (PDA) coating was achieved by using 4 mg/ml dopamine hydrochloride in 10 mM pH = 8.5 Tris buffer for 1 h with stirring before rinsing with Milli-Q water. For exosome coating, exosomes (10 μg in terms of protein) were incubated with PLA scaffold for 1 h at room temperature.

Exosome internalization study

Exosome internalization study was performed according to a previous study [25]. In brief, PKH26 red fluorescent cell linker kit for general cell membrane labeling was used to label exosomes onto PLA scaffold. Cells were seeded on 24-well tissue culture-treated coverslip overnight, then co-cultured with different scaffolds for

different time points (6 h and 24 h) at 37°C. Cells were washed with PBS, fixed with 4% paraformaldehyde, permeabilized using 0.25% Triton, and stained with Alexa Fluor 488-labeled phalloidin in dark for 1 h followed by DAPI staining. Images were captured using a confocal laser scanning microscope with a $\times 40$ objective (Leica DM IRB; Leica, Wetzlar, Germany).

Macrophage proliferation and live/dead assay

MTT cell proliferation assay was used as a metabolic activity indicator for cell viability. Briefly, Raw264.7 cells were seeded on 24-well tissue culture-treated cover slips overnight, then rinsed with PBS, then co-cultured with different scaffolds. On day 1 and day 3, 5 mg/ml 3-(4, 5-dimethylthiazol-2-yl)-2, 5-diphenyl tetrazolium bromide (MTT, Sigma, China) was added to the wells and incubated for additional 4 h at 37°C. One hundred micro-liter dimethyl sulfoxide (DMSO) was used to dissolve formazan generated during the incubation. The absorbance of the sample was measured using a microplate reader at 570 nm.

Live/dead staining was performed using staining solution containing 5 mg/mL FDA (fluorescein diacetate, green) and 2 mg/mL PI (propidium iodide, red) according to our previous study [22]. On day 1 and day 3, cells were incubated with the staining solution at room temperature. After washing with PBS, the samples were viewed using an inverted fluorescence microscope with a $\times 10$ objective (Leica, Wetzlar, Germany).

Macrophage polarization

Macrophages were activated with LPS as described previously [22]. Briefly, macrophages were seeded on 24-well tissue culture coverslip overnight, then stimulated with 1000 ng/ml of Lipopolysaccharide (LPS, *Escherichia coli* 0111: B4, Sigma, China) for 12 h. Cells were rinsed with PBS trice, then co-cultured with different scaffolds. After 24 h incubation, cells were washed with PBS, fixed with 4% paraformaldehyde, and stained with Alexa Fluor 594-labeled phalloidin for 1 h followed by DAPI staining. Images were acquired using a confocal laser scanning microscope with a $\times 40$ oil objective (Leica DM IRB; Leica, Wetzlar, Germany).

Reactive oxygen species (ROS)

Oxidative stress was achieved using hydrogen peroxide as previously described [26]. ROS levels were evaluated by DCFDA/H2DCFDA-Cellular ROS Assay Kit (Abcam, China) according to the manufacturer's instructions. Cells were stained with Hoechst 33342 and imaged using a confocal laser scanning microscope with a $\times 40$ oil objective (Leica DM IRB; Leica, Wetzlar, Germany). For the flow cytometric analysis of ROS levels, cells were

analyzed using a flow cytometer (BD Biosciences, Franklin Lakes, USA).

RNA isolation, reverse transcription, and real time PCR

Total RNA was isolated using TRIzol® reagent (15,596,018, Thermo Fisher Scientific, China). RNA concentration was measured by measuring the absorbance at 260 and 280 nm using NanoDrop 8000 spectrophotometer (NanoDrop technologies). cDNA was synthesized from 500 ng of total RNA sample using a RevertAid First Strand cDNA Synthesis Kit (K1622, Thermo Fisher Scientific, China). Real time PCR was performed using SYBR Green qPCR Master Mix (Life Technologies, China) on an ABI Prism 7500 Thermal Cycler (Applied Biosystems, Foster City, California, USA). The mRNA expression of the genes of interest was normalized against the housekeeping gene GAPDH. The difference between the mean Ct values of the gene of interest and the housekeeping gene was labelled ΔCt and the relative expression was calculated using the comparative Ct ($2^{-\Delta Ct}$) method [27].

hBMSC viability and live/dead assay

MTT cell proliferation assay and live/dead staining were used to assess cell viability as described above.

Immunofluorescent staining and confocal microscopy

Immunofluorescent staining of Alkaline phosphatase (ALP) was used to assess osteoblastic maturation of hBMSCs after 14 days of culture in osteogenic medium. Briefly, hBMSCs were washed with PBS twice and fixed with 4% paraformaldehyde for 10 min at room temperature. Cells were permeabilized with 0.25% Triton X-100 for 10 min and blocked with 4% bovine serum albumin (BSA) for 1 h at room temperature. After rinsing with PBS twice, cells were incubated with rabbit polyclonal to ALP (1:100, ab224335, Abcam) overnight at 4°C. The next day, cells were incubated with Fluorescein isothiocyanate-conjugated goat anti-rabbit IgG (H + L) secondary antibody for 1 h. Cells were counterstained with Alexa Fluor 594-labeled phalloidin followed by DAPI staining as described above. Images were acquired using a confocal laser scanning microscope with a $\times 40$ objective (Leica DM IRB; Leica, Wetzlar, Germany).

ALP and alizarin red S staining

ALP staining was also used to assess osteoblastic differentiation of hBMSCs after 14 days of culture in osteogenic medium. ALP staining was performed using BCIP/NBT Alkaline phosphatase Color Development Kit according to the manufacturer's instruction (Beyotime, Shanghai, China). Images were taken using inverted light microscope with a $\times 10$ objective (Leica, Wetzlar, Germany).

For the alizarin red staining, hBMSCs under osteoblastic differentiation were washed with PBS twice, then fixed by 4% paraformaldehyde for 20 min at room temperature. After fixation, the cells were then stained with 2% Alizarin Red S staining solution (pH = 4.1) for 30 min at room temperature. Images were taken using inverted light microscope with a $\times 10$ objective (Leica, Wetzlar, Germany). Quantification of Alizarin Red S staining was performed according to previous study [28].

Proteome profiler human XL cytokine array

Human XL cytokine array (Proteome Profiler Human XL cytokine arrays, ARY022, R&D Systems) was performed according to manufacturer's instruction. hBMSCs were co-cultured with PLA or PLA-Exo scaffold for 3 days in osteogenic medium. Membranes were incubated with collected supernatant at 4°C overnight. After a thorough washing, the membranes were incubated with a detection antibody cocktail for 1 h at room temperature and treated with streptavidin-horseradish peroxidase (HRP) solution for 30 min. The signal was visualized using enhanced chemiluminescence detection system and exposed to X-ray films. Images were captured and semi-quantified in the ImageJ software to determine the integrated density value of each protein spot on the grayscale.

Statistical analysis

All data were expressed as mean \pm standard deviations (SD, $n=3$). Statistical analysis was performed using GraphPad Prism 7 (Version 7.02) for Windows (GraphPad Software Inc., USA). Statistical differences between groups were determined with one-way analysis of variance (ANOVA) with Bonferroni's multiple comparison tests. A value of $p < 0.05$ was considered statistically significant.

Results and discussion

Characterization of exosomes extracted from hBMSCs

Despite the inherent tissue regenerative ability of hBMSCs, soluble factors secreted by MSCs, especially exosomes, have been indicated to play an important role in promoting tissue regeneration [29]. Due to their high therapeutic potential and their ability to transfer bioactive molecules, exosomes were firstly isolated from hBMSCs and were then used in this study to fabricate bio-inert PLA scaffold [29]. Exosomes were obtained from the conditioned medium of hBMSCs as previously described [22]. So far, various isolating methods have been developed to increase the yield of exosomes, including ultracentrifuge [30], commercial kits-based isolating method [31], ultrafiltration and precipitation [32], etc. Here, we used ultracentrifugation to isolate MSC-Exo from conditioned medium based on our established

protocol [22]. To validate successful isolation of MSCs-derived exosomes, we used two different methods: TEM and western blot detecting exosomal marker. The isolated exosomes were first detected by TEM. As shown in Fig. 1A, TEM analysis of exosomes extracted from hBMSCs showed spherical or cup-shaped morphology, which is consistent with our previous result [22] and other people's results [33, 34]. The western blotting result showed that isolated exosomes express significant levels of classical exosomal protein marker (CD63). (Fig. 1B).

To evaluate internalization of isolated exosomes into recipient cells, exosomes were labeled with PKH26 (red fluorescence) as described previously [35]. The mechanism of exosomes internalization into recipient cells remains a matter of debate, and several mechanisms have been proposed, including clathrin-dependent endocytosis, micropinocytosis, and caveolae-mediated endocytosis, etc. [36]. Raw 264.7 cells were incubated with PKH26-labeled exosomes for 24 h. The results from flow cytometry showed that macrophages treated with isolated exosomes demonstrated increased intracellular fluorescence signal, indicating that MSCs-Exo were uptake by RAW264.7 cells (Fig. 1C-D). Additionally, flow cytometry results also confirmed RAW264.7 cells have the higher uptake values compared to hBMSCs (Fig. 1E-F). It is also important to note that the uptake mechanism of exosomes from same origin is mainly recipient cells dependent, which exosomes released from donor cells are non-selectively incorporated into recipient cells [37]. We further used confocal microscopy to validate MSC-Exo internalization into recipient cells. As shown in Fig. 1G, PKH26 signal can be seen clearly around perinuclear areas in hBMSCs.

Preparation of bioactive exosome-functionalized scaffolds
Cylindrical discs of PLA scaffolds with a nearly 55% porosity were firstly fabricated. Figure 2A shows a light microscopy image of a 3D printed PLA scaffold before MSC-Exo fabrication. The binding between MSC-Exo and 3D printed PLA scaffold were validated using a confocal laser scanning microscopy (Fig. 2B).

To examine the cellular internalization of released exosomes from PLA-Exo scaffold into recipient cells, PKH26-labeled exosomes were used for scaffold fabrication. It was noted that the red fluorescence signal

increased dramatically at 24 h post-incubation in Raw 264.7 and hBMSCs, indicating good internalization of MSC-Exo from PLA-Exo scaffold into recipient cells (Fig. 2C&D).

Macrophage viability and morphology

To evaluate the viability of macrophages under the influence of different scaffolds, MTT cell proliferation assay was performed at different timepoints. It was reported that bone marrow aspirate MSCs-derived exosomes have a negative impact on the proliferation of activated peripheral blood mononuclear cells, and isolated B and T lymphocyte [38]. Abnormal proliferation of transforming growth factor (TGF)- β 1-stimulated bronchial smooth muscle cell was also reduced following MSC-derived exosomes treatment [39]. Additionally, in a rat ischemia-reperfusion injury model, MSC-derived exosomes treatment was found to improve tubular epithelial cell proliferation [40]. Here, MTT assay results indicated that exposure of macrophages with PLA-Exo scaffold did not affect cell viability on day 1 (Fig. 3A). After 72 h of culture, MTT absorbance significantly increased among all groups, which showed no difference (Fig. 3C). These results indicated that no significant cytotoxicity of PLA/Exo scaffold on macrophages.

The viability and proliferation of macrophages under the influence of different scaffolds were then assessed using live/dead staining at different timepoints. Figure 3 B&D shows the fluorescence images of live and dead macrophages after co-culturing with different scaffolds for 1 day and 3 days. Macrophages cultured with PLA-Exo showed similar pattern and morphology as in groups without exosomes. When the cells were cultured for 3 days, the cell numbers significantly increased in all groups, while dead cells numbers showed similar pattern in the presence of exosomes as in groups without exosomes.

Regulation of pro-inflammatory macrophages using PLA-Exo scaffolds

Macrophages are central phagocytic cells play an important role both in innate and adaptive immunity [41]. As important regulator to maintain normal tissue homeostasis, macrophages are located in almost all tissues with high plasticity and diversity [42]. Previous

(See figure on next page.)

Fig. 1 Characterization of hBMSCs-derived exosomes. **A** Morphological characterization of MSCs-derived exosomes with uranyl acetate negative staining. Isolated exosomes exhibited a cup-shaped morphology. **B** Western blot analysis of exosomal surface marker. Exosomes were found to be enriched for the exosomal surface marker CD63. **C** Flow cytometry analysis of exosome internalization into RAW264.7 cells. **D** The mean fluorescence intensity (MFI) obtained from RAW264.7 cells treated with or without MSC-Exo. **E** Internalization of MSC-Exo into hBMSCs. Cellular internalization of MSC-Exo by flow cytometric analysis. **F** MFI quantification of hBMSCs after 24 h of incubation with isolated exosomes. **G** Uptake of exosomes released from MSC-Exo by hBMSCs. Exosomes were prelabeled with PKH26. The internalization of the exosomes was evaluated by a confocal laser scanning microscopy

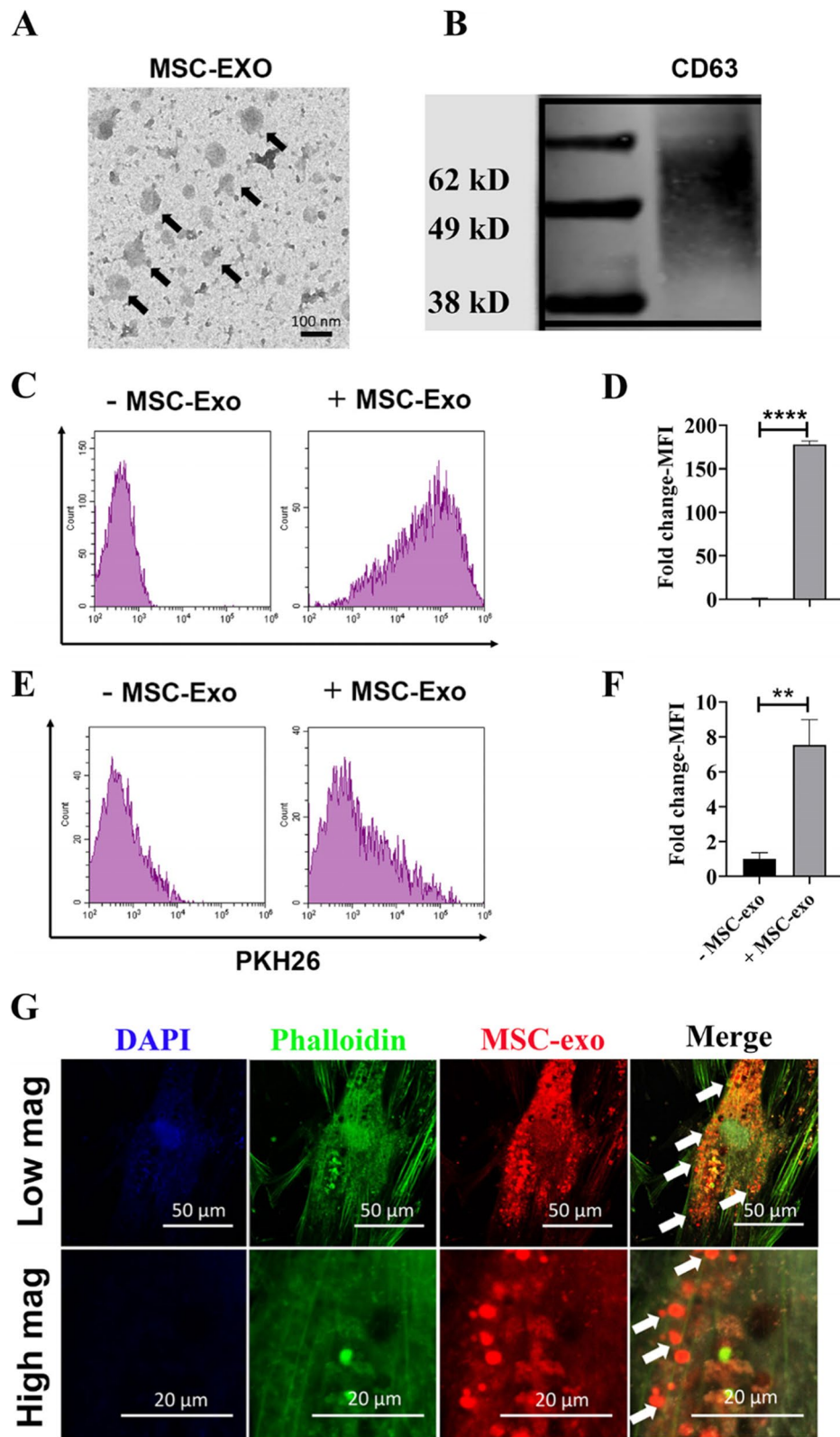


Fig. 1 (See legend on previous page.)

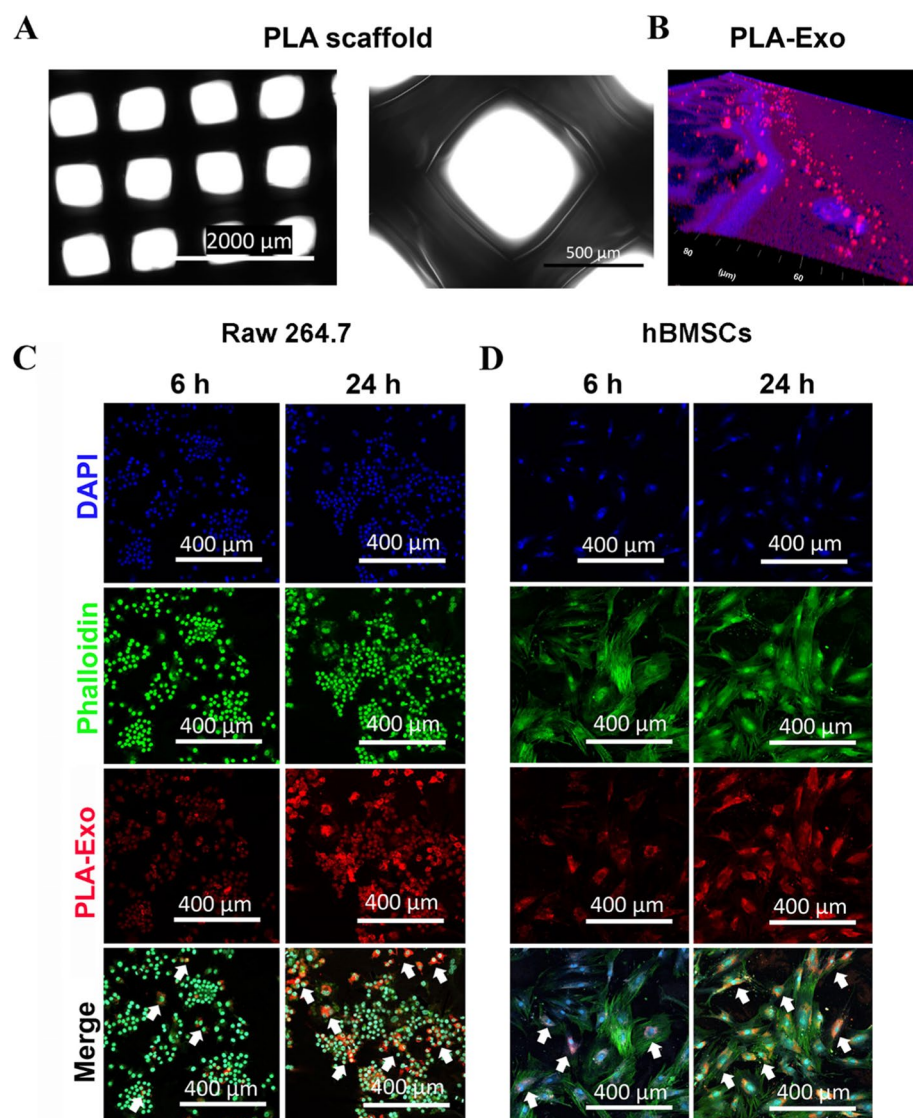
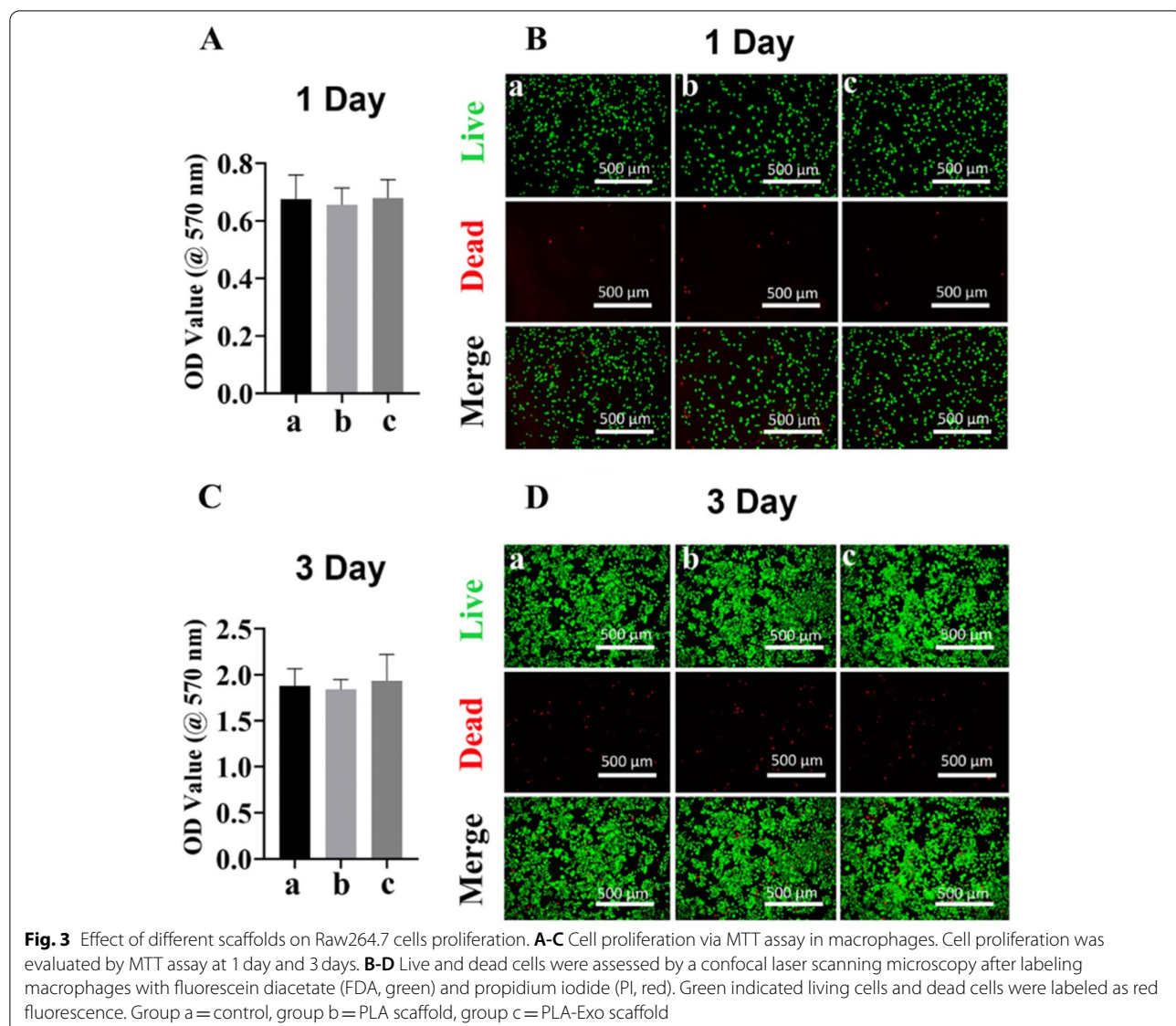


Fig. 2 Fabrication of PLA-Exo scaffold. **A** The view of the 3D printed PLA scaffold. **B** Representative imaging of PLA scaffold modified with PKH26-labeled exosomes. **C** Fluorescent imaging of exosomes released from PLA-Exo scaffold into Raw 264.7 cells. Cells were stained with phalloidin (green), nucleus (blue), and examined by a confocal laser scanning microscope. **D** Uptake of exosomes released from PLA-Exo scaffold by hBMS Cs. Exosomes were prelabeled with PKH26. The internalization of the exosomes released from scaffold was evaluated by a confocal laser scanning microscope

studies indicated resident osteal macrophages as well as migrated macrophages into the bone healing side have a major impact on the effective bone repair [43, 44]. Macrophages are generally divided into pro-inflammatory M1 and anti-inflammatory M2 types of based on their polarization states [45], which pro-inflammatory macrophages predominant the first stage of fracture healing while anti-inflammatory macrophages are abundantly detected in later stage of bone regeneration [46]. Excessive acute and chronic inflammation, caused by microbial infection, trauma, and autoimmune diseases, etc.

lead to the persistent inflammatory state and excessive production of pro-inflammatory cytokines [47], which in turn, resulting in increased bone resorption and suppression of bone formation [47].

To examine the pro-inflammatory macrophage internalization of released exosomes, PKH carbocyanine dye-labeled exosomes were used for scaffold fabrication as mentioned above, and a confocal laser scanning microscopy was used for observation. As shown in Fig. 4A, PKH26 signal can be seen clearly around peri-nuclear areas in pro-inflammatory macrophages after



24 hours of culturing, which is consistent with previous study [48].

The macrophage morphology was then examined microscopically using a confocal laser scanning microscopy, focusing on the center regions of the samples. LPS

predominantly polarizes macrophages to pancake-like shape after stimulation, with increased cellular areas and the number of processes. Previous studies indicated that pro-inflammatory M1 macrophages appeared large, round-shape morphology, while anti-inflammatory M2

(See figure on next page.)

Fig. 4 Effect of different scaffolds on the inflammatory macrophage polarization. **A** Confocal microscopy imaging of exosomes released from PLA-Exo scaffold internalization into pro-inflammatory macrophages. Cells were stained with DAPI (blue) and examined by a confocal laser scanning microscopy. **B** Representative confocal microscopy images of pro-inflammatory macrophages response to different scaffolds. Cells were fixed, stained for phalloidin (red), nuclei (blue) and visualized by a confocal laser scanning microscopy. **C** Representative CLSM images showing the changes of intracellular ROS levels. Nuclei were stained with Hoechst 33342 (blue). **D** ROS intensity detection using flow cytometry. Intracellular ROS levels decrease following PLA-Exo scaffold treatment: *** $p < 0.0001$. **E** qRT-PCR results of relative gene expression of pro-inflammatory cytokine. The values were normalized to GAPDH as a housekeeping gene. Significant difference (* $p < 0.05$, *** $p < 0.0001$). Group a = control, group b = PLA scaffold, group c = PLA-Exo scaffold

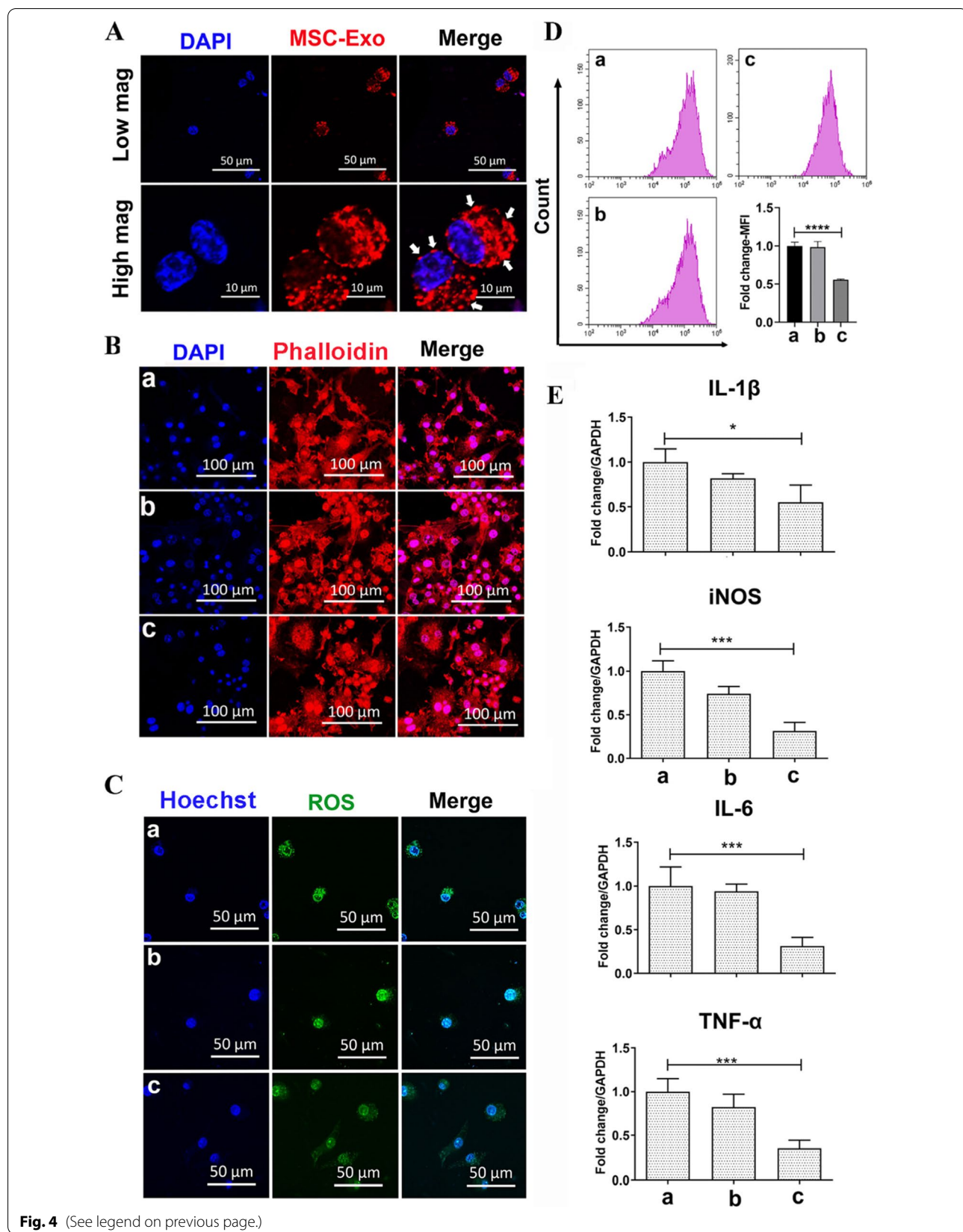


Fig. 4 (See legend on previous page.)

macrophages showed elongated shape [49, 50]. Here, given the plasticity of macrophages, a hybrid morphology with both elongated and pancake-like shape can be seen (Fig. 4B).

Reactive oxygen species (ROS) and oxidative stress play an important role in a number of physiological and pathological conditions, including age-induced loss of bone mass and osteoporosis [51]. ROS act as one of the key molecules that regulate inflammatory signaling [52]. Therefore, we first examined the effects of PLA-Exo on ROS production in oxidative stress damage in macrophages by flow cytometry analysis. To examine ROS production, we used fluorescence staining following 2',7'-dichlorodihydrofluorescein diacetate (DCFH-DA) staining. As shown in Fig. 4C, the intensities of green fluorescence in PLA-Exo scaffold group were significantly lower than those from control groups without exosome fabrication, indicating that the intracellular ROS level was reduced following PLA-Exo scaffold treatment. Xia et al. investigated the effect of MSCs-derived exosomes on H₂O₂-induced nucleus pulposus cell and found a significant reduction of ROS levels following exosome treatment [53]. In another study, MSCs-derived exosomes also decreased the levels iNOS expression and NO production IL-1 β challenged chondrocytes [54]. To further validate our results, we used flow cytometry analysis. The results indicated that culture of oxidative stress-related macrophages with PLA-Exo scaffold significantly reduces relative ROS production (Fig. 4D).

We used qRT-PCR to determine the relative gene expression of pro-inflammatory cytokine after culturing with different scaffolds. Pro-inflammatory M1 macrophages are characterized by the high expression of inflammatory cytokines and [55]. As shown in Fig. 4E, IL-1 β , iNOS, IL-6, and TNF- α gene expression levels were significantly decreased in PLA-Exo group compared with groups without exosome fabrication. Which is consistent with the anti-inflammatory effect reported in literature [56]. These results indicated that immunoregulatory role of PLA-Exo scaffold on pro-inflammatory response.

hBMSC viability and morphology

The biocompatibility of different scaffolds with hBMSCs was investigated using MTT cell proliferation assay at different timepoints. Previous study indicated that MSCs-derived exosomes could induce a dose-dependent increase of normal adult and diabetic wound fibroblasts proliferation and migration in vitro [57]. MSCs-derived exosomes have also been reported to enhance cell viability and proliferation in various cell-based models [58]. As shown in Figs. 5A&C, MTT assay results indicated that co-culture of hBMSCs with PLA-Exo scaffold showed no

toxicity on day 3 and day 5. Sue l al. reported that both MSCs-derived exosomes and MSCs exosome immobilized PEI-modified electrospun fibers showed no stimulative effect on the proliferation of isolated T cells in vitro [59], which is consistent with our results. Our study also supported by the results from Qin et al., indicating marginal effect of MSCs-derived exosomes on osteoblast proliferation by flow cytometry analysis and MTT assay [60]. These results indicate that PLA-Exo scaffolds are highly biocompatible for hBMSCs growth.

We then performed live/dead staining to further assess cell proliferation after 3day and 5days culture. Figure 5B&D show hBMSCs had a homogeneous distribution and growth pattern in all groups. High viability of hBMSCs was also observed after culturing with PLA-Exo scaffold.

Osteogenic differentiation of hBMSCs under the influence of PLA-Exo scaffolds

To evaluate the effect of PLA-Exo scaffold on the osteogenic differentiation of hBMSCs, we first evaluated the expression of ALP activity by using ALP staining. As an early expression marker associated with osteoblastic differentiation, ALP plays an important role in bone mineralization and skeletal development [61]. The effect of MSCs-derived exosomes on osteoblastic differentiation in vitro and in vivo were also reported [60, 62]. The ALP staining result is presented in Fig. 5A. The results indicated that PLA-Exo scaffold markedly increased ALP levels in hBMSCs compared to the control group after osteogenic induction for 14days. To further evaluate the osteoblastic maturation of hBMSCs induced by the PLA-Exo scaffold, fluorescence staining was used to measure ALP expression, which were labeled with green fluorescence. As shown in Fig. 6B, the fluorescence intensity of ALP was significantly higher in hBMSCs treated with PLA-Exo scaffold compared with the rest groups.

The expression profile of osteogenic differentiation marker genes in hBMSCs were assessed using qRT-PCR. As shown in Fig. 6C, gene expressions of ALP, OCN, Runx2, and IBSP were examined, normalized by GAPDH. hBMSCs cultured with PLA-Exo scaffold expressed higher levels of transcription gene (Runx2). As one of the most important osteogenic transcription factors, Runx2 is crucial for the differentiation and maturation of MSCs [63]. hBMSCs treated with PLA-Exo scaffold also showed significant increase of the ALP mRNA expression, confirming the results of ALP staining and ALP fluorescence staining. In general, the gene expression levels of the other osteogenic differentiation markers (OCN and IBSP) also showed the same trend.

To understand the effect of PLA-Exo scaffold on the regulation of cytokines/chemokines secretion in

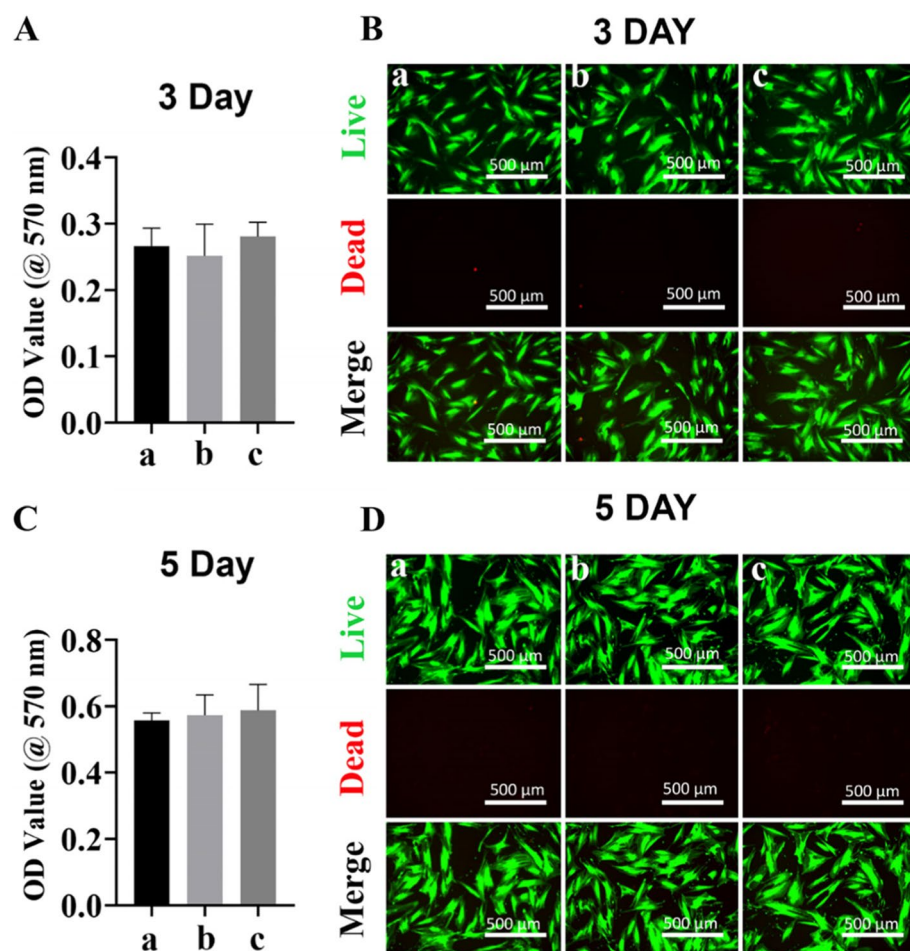


Fig. 5 Cell proliferation analysis in hBMSCs. **A-C** Cell proliferation analysis. Cell viability was evaluated by MTT assay at 3 days and 5 days. **B-D** Live and dead assay of hBMSCs co-cultured with different scaffolds for 3 day and 5 days. The cells were stained with fluorescein diacetate (FDA, green) and propidium iodide (PI, red) and were examined by a confocal microscopy. Green indicated living cells and dead cells were labeled as red fluorescence. Group a = control, group b = PLA scaffold, group c = PLA-Exo scaffold

hBMSCs, we performed cytokine array analysis. The expression of angiopoietin-1, endoglin, IGFBP-3, IL-8, MCP-1, and SDF-1 α were significantly increased in PLA-Exo group (Fig. 6D&E). Suzuki et al. found that overexpression of angiopoietin-1 in osteoblasts enhanced bone mass in angiopoietin-1-transgenic mice [64]. In addition, SDF-1 α was reported involving in osteogenesis and

angiogenesis, which its overexpression promoted bone regeneration in osteonecrotic femoral head [65].

To further validate the effect of PLA-Exo scaffold on the osteogenic differentiation of hBMSCs, matrix mineralization was assessed by Alizarin Red S staining. As shown in Fig. 6F, hBMSCs cultured with PLA-Exo scaffold exhibited more intense staining for calcium

(See figure on next page.)

Fig. 6 Osteogenic differentiation capacity of hBMSCs stimulated. **A** ALP staining images of hBMSCs cultured with different scaffolds at days 14. PLA-Exo scaffold improves the expression of ALP. **B** Immunofluorescence staining for osteogenic differentiation marker (ALP) in hBMSCs cultured with different scaffolds for 14 days. Cells were fixed, stained for ALP (green), phalloidin (red), and nuclei (blue), and examined by a confocal laser scanning microscopy. **C** Gene expression of osteogenesis-specific markers by qRT-PCR. Significant difference ** $p < 0.01$, *** $p < 0.001$. **D** Representative images for cytokine array assay. hBMSCs were cultured with PLA or PLA-Exo scaffold for 3 days, and the cell culture supernatant were collected for human proteome XL cytokine array. **E** Quantification of cytokine array assay. Significant difference: * $p < 0.05$, ** $p < 0.01$, *** $p < 0.001$. **F** Alizarin red S staining for calcium nodules formation at 21 days. **G** Calcium nodules formation was eluted and measured using a microplate reader at 405 nm. Significant difference: **** $p < 0.0001$. Group a = control, group b = PLA scaffold, group c = PLA-Exo scaffold

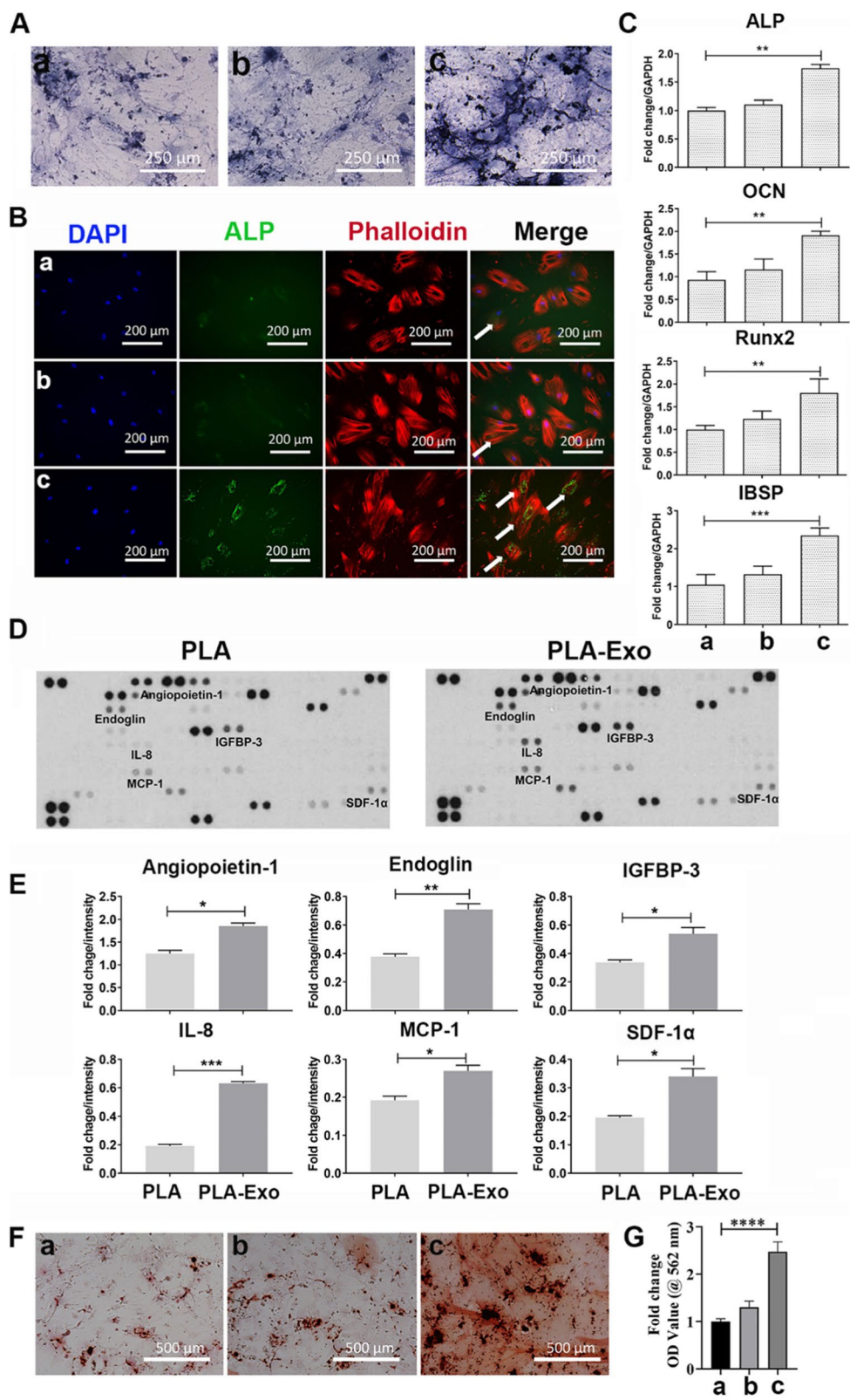


Fig. 6 (See legend on previous page.)

deposition. Consistently, quantification of the intensity of alizarin red S staining also indicated marked increase of calcium concentration in PLA-Exo scaffold (Fig. 6G).

Conclusion

In the current study, a bioactive 3D porous PLA scaffold modified with MSC-Exo was fabricated to examine its roles in regulating inflammation and improving the osteogenic differentiation in hBMSCs. The bio-functionality of the original PLA scaffold was greatly improved by loading MSC-Exo, as evidenced by significant reduction of the pro-inflammatory markers and ROS production in inflammatory macrophages. Furthermore, the *in vitro* osteogenesis study further revealed high expression of osteoblastic markers and mineralization, indicating the pro-osteogenic effect of our bioactive 3D porous PLA scaffold. In the future, more studies, including the *in vivo* study, are necessary to further validate its bio-functionality.

Acknowledgments

Not applicable.

Authors' contributions

All authors made substantial contributions to conception and design, acquisition of the data, or analysis and interpretation of the data; took part in drafting the article or revising it critically for important intellectual content; gave final approval of the version to be published; and agreed to be accountable for all aspects of the work.

Funding

This work was financially supported by the National Natural Science Foundation of China (Grant No. 86060620 and 31960209), Guizhou Science and Technology Fund Project (Grant No. [2020]1Y093), Zunyi Science and Technology Fund Project (Grant No. Zunyi Kehe HZ Zi [2021]40), and Doctoral Science Research Startup Funding of Zunyi Medical University (Grant No.F-934 and No.2017-01).

Availability of data and materials

Please contact author for data requests.

Declarations

Ethics approval and consent to participate

Not applicable.

Consent for publication

Not applicable.

Competing interests

The authors declare that they have no competing interests.

Author details

¹Department of Hygiene Toxicology, Zunyi Medical University, Zunyi 563000, Guizhou, China. ²Department of Orthopaedic Surgery, Affiliated Hospital of Zunyi Medical University, Zunyi 563003, Guizhou, China. ³School of Mechanical, Medical & Process Engineering, Centre for Biomedical Technologies, Queensland University of Technology (QUT), Brisbane, QLD 4000, Australia. ⁴Australia China Centre for Tissue Engineering and Regenerative Medicine, Kelvin Grove, Brisbane, Queensland 4059, Australia. ⁵Department of Pre-hospital Emergency, Central Hospital of Chongqing University / Chongqing Emergency Medical Center, Chongqing, Chongqing 400014, China.

Received: 3 May 2022 Accepted: 8 August 2022
Published online: 22 August 2022

References

- Roddy E, DeBaun MR, Daoud-Gray A, Yang YP, Gardner MJ. Treatment of critical-sized bone defects: clinical and tissue engineering perspectives. *Eur J Orthop Surg Traumatol.* 2018;28(3):351–62.
- Stahl A, Yang YP. Regenerative approaches for the treatment of large bone defects. *Tissue Eng Part B Rev.* 2021;27(6):539–47.
- Chen FM, Liu X. Advancing biomaterials of human origin for tissue engineering. *Prog Polym Sci.* 2016;53:86–168.
- Vidal L, Kampleitner C, Brennan M, Hoornaert A, Layrolle P. Reconstruction of large skeletal defects: current clinical therapeutic strategies and future directions using 3D printing. *Front Bioeng Biotechnol.* 2020;8:61.
- Dai J, Su Y, Zhong S, Cong L, Liu B, Yang J, et al. Exosomes: key players in cancer and potential therapeutic strategy. *Signal Transduct Target Ther.* 2020;5(1):145.
- Zhang Y, Liu Y, Liu H, Tang WH. Exosomes: biogenesis, biologic function and clinical potential. *Cell Biosci.* 2019;9:19.
- Kalluri R, LeBleu VS. The biology, function, and biomedical applications of exosomes. *Science.* 2020;367(6478):eaau6977.
- Corradietti B, Gonzalez D, Mendes Pinto I, Conlan RS. Editorial: Exosomes as therapeutic systems. *Front Cell Dev Biol.* 2021;9:714743.
- Zheng C, Chen J, Liu S, Jin Y. Stem cell-based bone and dental regeneration: a view of microenvironmental modulation. *Int J Oral Sci.* 2019;11(3):23.
- Arthur A, Gronthos S. Clinical application of bone marrow Mesenchymal stem/stromal cells to repair skeletal tissue. *Int J Mol Sci.* 2020;21(24):9759.
- Ma ZJ, Yang JJ, Lu YB, Liu ZY, Wang XX. Mesenchymal stem cell-derived exosomes: toward cell-free therapeutic strategies in regenerative medicine. *World J Stem Cells.* 2020;12(8):814–40.
- Nakamura Y, Miyaki S, Ishitobi H, Matsuyama S, Nakasa T, Kamei N, et al. Mesenchymal-stem-cell-derived exosomes accelerate skeletal muscle regeneration. *FEBS Lett.* 2015;589(11):1257–65.
- Zhang S, Chuah SJ, Lai RC, Hui JHP, Lim SK, Toh WS. MSC exosomes mediate cartilage repair by enhancing proliferation, attenuating apoptosis and modulating immune reactivity. *Biomaterials.* 2018;156:16–27.
- Furuta T, Miyaki S, Ishitobi H, Ogura T, Kato Y, Kamei N, et al. Mesenchymal stem cell-derived Exosomes promote fracture healing in a mouse model. *Stem Cells Transl Med.* 2016;5(12):1620–30.
- Zhang J, Guan J, Niu X, Hu G, Guo S, Li Q, et al. Exosomes released from human induced pluripotent stem cells-derived MSCs facilitate cutaneous wound healing by promoting collagen synthesis and angiogenesis. *J Transl Med.* 2015;13:49.
- Tan CY, Lai RC, Wong W, Dan YY, Lim SK, Ho HK. Mesenchymal stem cell-derived exosomes promote hepatic regeneration in drug-induced liver injury models. *Stem Cell Res Ther.* 2014;5(3):76.
- Lai RC, Arslan F, Lee MM, Sze NS, Choo A, Chen TS, et al. Exosome secreted by MSC reduces myocardial ischemia/reperfusion injury. *Stem Cell Res.* 2010;4(3):214–22.
- Kaspi H, Semo J, Abramov N, Dekel C, Lindborg S, Kern R, et al. MSC-NTF (NurOwn®) exosomes: a novel therapeutic modality in the mouse LPS-induced ARDS model. *Stem Cell Res Ther.* 2021;12(1):72.
- Kordelas L, Rebmann V, Ludwig AK, Radtke S, Ruesing J, Doeppner TR, et al. MSC-derived exosomes: a novel tool to treat therapy-refractory graft-versus-host disease. *Leukemia.* 2014;28(4):970–3.
- Swetha S, Balagangadhara K, Lavanya K, Selvamurugan N. Three-dimensional-poly(lactic acid) scaffolds coated with gelatin/magnesium-doped nano-hydroxyapatite for bone tissue engineering. *Biotechnol J.* 2021;16(11):e2100282.
- Ashwin B, Abinaya B, Prasith TP, Chandran SV, Yadav LR, Vairamani M, et al. 3D-poly (lactic acid) scaffolds coated with gelatin and mucic acid for bone tissue engineering. *Int J Biol Macromol.* 2020;162:523–32.
- Lu H, Zhang Y, Xiong S, Zhou Y, Xiao L, Ma Y, et al. Modulatory role of silver nanoparticles and Mesenchymal stem cell-derived exosome-modified barrier membrane on macrophages and Osteogenesis. *Front Chem.* 2021;9:699802.
- Théry C, Witwer KW, Aikawa E, Alcaraz MJ, Anderson JD, Andriantsitohaina R, et al. Minimal information for studies of extracellular vesicles 2018

- (MISEV2018): a position statement of the International Society for Extracellular Vesicles and update of the MISEV2014 guidelines. *J Extracell Vesicles*. 2018;7(1):1535750.
24. Deng L, Pan X, Zhang Y, Sun S, Lv L, Gao L, et al. Immunostimulatory potential of MoS₂ Nanosheets: enhancing dendritic cell maturation, migration and T cell elicitation. *Int J Nanomedicine*. 2020;15:2971–86.
 25. Wei F, Li M, Crawford R, Zhou Y, Xiao Y. Exosome-integrated titanium oxide nanotubes for targeted bone regeneration. *Acta Biomater*. 2019;86:480–92.
 26. Lin W, Qi X, Guo W, Liang D, Chen H, Lin B, et al. A barrier against reactive oxygen species: chitosan/acellular dermal matrix scaffold enhances stem cell retention and improves cutaneous wound healing. *Stem Cell Res Ther*. 2020;11(1):383.
 27. Schmittgen TD, Livak KJ. Analyzing real-time PCR data by the comparative CT method. *Nat Protoc*. 2008;3(5):1101–8.
 28. Lee DJ, Tseng HC, Wong SW, Wang Z, Deng M, Ko CC. Dopaminergic effects on in vitro osteogenesis. *Bone Res*. 2015;3:15020.
 29. Zhang B, Tian X, Hao J, Xu G, Zhang W. Mesenchymal stem cell-derived extracellular vesicles in tissue regeneration. *Cell Transplant*. 2020;29:963689720908500.
 30. Kim JY, Rhim WK, Yoo YI, Kim DS, Ko KW, Heo Y, et al. Defined MSC exosome with high yield and purity to improve regenerative activity. *J Tissue Eng*. 2021;12:20417314211008626.
 31. Cambier L, Stachelek K, Triska M, Jubran R, Huang M, Li W, et al. Extracellular vesicle-associated repetitive element DNAs as candidate osteosarcoma biomarkers. *Sci Rep*. 2021;11(1):94.
 32. Chen J, Li P, Zhang T, Xu Z, Huang X, Wang R, et al. Review on strategies and Technologies for Exosome Isolation and Purification. *Front Bioeng Biotechnol*. 2022;9:811971.
 33. Xie L, Chen Z, Liu M, Huang W, Zou F, Ma X, et al. MSC-derived Exosomes protect vertebral endplate chondrocytes against apoptosis and calcification via the miR-31-5p/ATF6 Axis. *Mol Ther Nucleic Acids*. 2020;22:601–14.
 34. Liao Z, Luo R, Li G, Song Y, Zhan S, Zhao K, et al. Exosomes from mesenchymal stem cells modulate endoplasmic reticulum stress to protect against nucleus pulposus cell death and ameliorate intervertebral disc degeneration in vivo. *Theranostics*. 2019;9(14):4084–100.
 35. Dehghani M, Gulvin SM, Flax J, Gaborski TR. Systematic evaluation of PKH Labelling on extracellular vesicle size by nanoparticle tracking analysis. *Sci Rep*. 2020;10(1):9533.
 36. Zheng Y, Tu C, Zhang J, Wang J. Inhibition of multiple myeloma-derived exosomes uptake suppresses the functional response in bone marrow stromal cell. *Int J Oncol*. 2019;54(3):1061–70.
 37. Horibe S, Tanahashi T, Kawauchi S, Murakami Y, Rikitake Y. Mechanism of recipient cell-dependent differences in exosome uptake. *BMC Cancer*. 2018;18(1):47.
 38. Khare D, Or R, Resnick I, Barkatz C, Almogi-Hazan O, Avni B. Mesenchymal stromal cell-derived Exosomes affect mRNA expression and function of B-lymphocytes. *Front Immunol*. 2018;9:3053.
 39. Shan L, Si Liu, Q Zhang, Q Zhou, Y Shang. Human bone marrow-mesenchymal stem cell-derived exosomal microRNA-188 reduces bronchial smooth muscle cell proliferation in asthma through suppressing the JARID2/Wnt/β-catenin axis. *Cell Cycle*. 2022;21(4):352–67.
 40. Gatti S, Bruno S, Dereibus MC, Sordi A, Cantaluppi V, Tetta C, et al. Microvesicles derived from human adult mesenchymal stem cells protect against ischaemia-reperfusion-induced acute and chronic kidney injury. *Nephrol Dial Transplant*. 2011;26(5):1474–83.
 41. Ley K, Pramod AB, Croft M, Ravichandran KS, Ting JP. How mouse macrophages sense what is going on. *Front Immunol*. 2016;7:204.
 42. Hirayama D, Iida T, Nakase H. The phagocytic function of macrophage-enforcing innate immunity and tissue homeostasis. *Int J Mol Sci*. 2017;19(1):92.
 43. Sinder BP, Pettit AR, McCauley LK. Macrophages: their emerging roles in bone. *J Bone Miner Res*. 2015;30(12):2140–9.
 44. Schlundt C, El Khassawna T, Serra A, Dienelt A, Wendler S, Schell H, et al. Macrophages in bone fracture healing: their essential role in endochondral ossification. *Bone*. 2018;106:78–89.
 45. Niu Y, Wang Z, Shi Y, Dong L, Wang C. Modulating macrophage activities to promote endogenous bone regeneration: biological mechanisms and engineering approaches. *Bioact Mater*. 2021;6(1):244–61.
 46. Wu AC, Raggatt LJ, Alexander KA, Pettit AR. Unraveling macrophage contributions to bone repair. *Bonekey Rep*. 2013;2:373.
 47. Maruyama M, Rhee C, Utsunomiya T, Zhang N, Ueno M, Yao Z, et al. Modulation of the inflammatory response and bone healing. *Front Endocrinol (Lausanne)*. 2020;11:386.
 48. Bouchareychas L, Duong P, Covarrubias S, Alsop E, Phu TA, Chung A, et al. Macrophage Exosomes resolve atherosclerosis by regulating hematopoiesis and inflammation via MicroRNA cargo. *Cell Rep*. 2020;32(2):107881.
 49. Rostam HM, Reynolds PM, Alexander MR, Gadegaard N, Ghaemmaghami AM. Image based machine learning for identification of macrophage subsets. *Sci Rep*. 2017;7(1):3521.
 50. Vereijken EJ, Heijnen PD, Baron W, de Vries EH, Dijkstra CD, Teunissen CE. Classically and alternatively activated bone marrow derived macrophages differ in cytoskeletal functions and migration towards specific CNS cell types. *J Neuroinflammation*. 2011;8:58.
 51. Tai TW, Chen CY, Su FC, Tu YK, Tsai TT, Lin CF, et al. Reactive oxygen species are required for zoledronic acid-induced apoptosis in osteoclast precursors and mature osteoclast-like cells. *Sci Rep*. 2017;7:44245.
 52. Forrester SJ, Kikuchi DS, Hernandes MS, Xu Q, Griendl KK. Reactive oxygen species in metabolic and inflammatory signaling. *Circ Res*. 2018;122(6):877–902.
 53. Xia C, Zeng Z, Fang B, Tao M, Gu C, Zheng L, et al. Mesenchymal stem cell-derived exosomes ameliorate intervertebral disc degeneration via anti-oxidant and anti-inflammatory effects. *Free Radic Biol Med*. 2019;143:1–15.
 54. Tofiño-Vian M, Guillén MI, Pérez Del Caz MD, Silvestre A, Alcaraz MJ. Microvesicles from human adipose tissue-derived Mesenchymal stem cells as a new protective strategy in osteoarthritic chondrocytes. *Cell Physiol Biochem*. 2018;47(1):11–25.
 55. Oishi Y, Manabe I. Macrophages in inflammation, repair and regeneration. *Int Immunol*. 2018;30(11):511–28.
 56. Arabpour M, Saghazadeh A, Rezaei N. Anti-inflammatory and M2 macrophage polarization-promoting effect of mesenchymal stem cell-derived exosomes. *Int Immunopharmacol*. 2021;97:107823.
 57. Shabbir A, Cox A, Rodriguez-Menocal L, Salgado M, Van Badiavas E. Mesenchymal stem cell Exosomes induce proliferation and migration of Normal and chronic wound fibroblasts, and enhance angiogenesis in vitro. *Stem Cells Dev*. 2015;24(14):1635–47.
 58. Quiñones-Vico MI, Sanabria-de R, la Torre M, Sánchez-Díaz Á-S, Montero-Vilchez T, Fernández-González A, et al. The role of Exosomes derived from Mesenchymal stromal cells in dermatology. *Front Cell Dev Biol*. 2021;9:647012.
 59. Su N, Hao Y, Wang F, Hou W, Chen H, Luo Y. Mesenchymal stromal exosome-functionalized scaffolds induce innate and adaptive immunomodulatory responses toward tissue repair. *Sci Adv*. 2021;7(20):eabf7207.
 60. Qin Y, Wang L, Gao Z, Chen G, Zhang C. Bone marrow stromal/stem cell-derived extracellular vesicles regulate osteoblast activity and differentiation in vitro and promote bone regeneration in vivo. *Sci Rep*. 2016;6:21961.
 61. Sato M, Saitoh I, Kiyokawa Y, Iwase Y, Kubota N, Ibano N, et al. Tissue-nonspecific alkaline phosphatase, a possible mediator of cell maturation: towards a new paradigm. *Cells*. 2021;10(12):3338.
 62. Wang X, Omar O, Vazirisan F, Thomsen P, Ekström K. Mesenchymal stem cell-derived exosomes have altered microRNA profiles and induce osteogenic differentiation depending on the stage of differentiation. *PLoS One*. 2018;13(2):e0193059.
 63. Xu J, Li Z, Hou Y, Fang W. Potential mechanisms underlying the Runx2 induced osteogenesis of bone marrow mesenchymal stem cells. *Am J Transl Res*. 2015;7(12):2527–35.
 64. Sacks D, Baxter B, Campbell BCV, Carpenter JS, Cognard C, Dippel D, et al. Multisociety consensus quality improvement revised consensus statement for endovascular therapy of acute ischemic stroke. *Int J Stroke*. 2018;13(6):612–32.
 65. Yang F, Xue F, Guan J, Zhang Z, Yin J, Kang Q. Stromal-cell-derived factor (SDF) 1-alpha overexpression promotes bone regeneration by Osteogenesis and angiogenesis in osteonecrosis of the femoral head. *Cell Physiol Biochem*. 2018;46(6):2561–75.

Publisher's Note

Springer Nature remains neutral with regard to jurisdictional claims in published maps and institutional affiliations.